Journal of Nuclear Materials 407 (2010) 100–109

Contents lists available at ScienceDirect

Journal of Nuclear Materials

journal homepage: www.elsevier.com/locate/jnucmat

Effect of helium on the microstructure of spent fuel in a repository: An operational approach

Cécile Ferry [a,*], Jean-Paul Piron [b], Antoine Ambard [c]

[a] Commissariat à l'Energie Atomique (CEA), Nuclear Energy Division, Department of Physico-Chemistry, CEA-Saclay, PC 40, 91191 Gif-sur-Yvette, France
[b] Commissariat à l'Energie Atomique (CEA), Nuclear Energy Division, Department of Nuclear Fuel Studies, CEA-Cadarache, 13108 Saint-Paul Lez Durance, France
[c] Electricité de France (EDF), R&D Division, Les Renardières, 77818 Morez-sur-Loing, France

ARTICLE INFO

Article history:
Received 9 July 2010
Accepted 22 September 2010

ABSTRACT

In a repository, the release of radionuclides from spent fuel rods will strongly depend on the pellet microstructure existing when water comes into contact with the spent fuel surface, i.e. after 10,000 years of disposal. During this period, a large quantity of He atoms is produced by α-disintegrations of actinides in the spent fuel. A conservative model is proposed here to evaluate the consequences of He on the spent fuel microstructure. According to the solubility and diffusion properties of He under repository conditions, two scenarios are considered: He atoms can be trapped in fission gas bubbles or form new bubbles. In spite of the conservative assumptions of the model, the calculated values of bubble or pore pressure are much lower than critical values derived from rupture criteria. No evolution of the microstructure of the spent UO_2 fuel is thus expected before the breaching of the canister.

1. Introduction

Radionuclide release from spent fuel rods under disposal conditions is classically composed of two contributions. The first contribution is a rapid release of some radionuclides (Cs, I, Se and to a lesser extent Sr), when water comes into contact with the spent fuel surface. The second contribution is a slow long-term release of the radionuclides that are embedded in the spent fuel matrix at the end of irradiation. In this case, the kinetics of release are governed by the spent fuel matrix dissolution as a consequence of water radiolysis and competing effect of reducing agents from the canister or the clay.

The rapid release of radioactivity is quantified as the Instant Release Fraction (IRF). The IRF includes all the radionuclides, which are located in the spent fuel rod regions with anticipated low confinement properties at the arrival of water, i.e. about 10,000 years after the beginning of disposal [1]. Many questions arise from this definition: which zones will contribute to the IRF after 10,000 years of evolution in the tight container? How will the spent fuel microstructure evolve before water access, due to thermal decrease and residual radioactivity?

Studies of spent nuclear fuel (SNF) evolution in a closed system (i.e. no matter exchange with the exterior) have concluded that the evolution of the pellet microstructure will strongly depend on He fate in the SNF [2]. Table 1 gives the concentration of He in spent UO_2 fuels as a function of time.

This paper focuses on He fate in spent fuel in repository and the effects on the initial microstructure of the SNF pellet.

Experimental data whose aim is to determine the diffusion coefficient of He in UO_2 bring some insight on the behaviour of He in UO_2 during a thermal treatment.

Roudil et al. [3] have measured the thermal diffusion of He in UO_2 disks implanted with He at various fluences. The maximal concentration of He, reached at a depth of around 6.5 μm, varied between 0.06 and 0.6 at.%. A lower value of the diffusion coefficient was measured at the high fluence of implantation and is expected to be due to the precipitation of He atoms in bubbles. However the energy of activation was the same for both fluences.

Martin et al. [4] have studied He fate in sintered UO_2 disks during heavy ion bombardment and thermal treatment at high temperature (800 °C and 1100 °C). In these experiments, the maximal He concentration (0.3 at.%) was achieved at a depth of about 2 μm. The apparent diffusion coefficients derived from the measured profiles were consistent with the values obtained at a lower concentration of implantation. Therefore, these observations do not evidence any detrimental effect of He implantation.

Guilbert et al. [5] have measured He profiles in UO_2 disks after a thermal treatment of one hour at temperatures of 500 °C and 600 °C. The maximal He concentration was 1.1 at.% at 1.9 μm from the sample surface. The authors observed a flaking phenomenon after thermal treatment, which seems to be caused by He bubble

* Corresponding author. Address: CEA-Saclay, Nuclear Energy Division, Department of Physico-Chemistry, Bâtiment 450, PC 40, 91191 Gif-sur-Yvette, France. Tel.: +33 (0) 1 69 08 83 65; fax: +33 (0) 1 69 08 32 42.
E-mail address: cecile.ferry@cea.fr (C. Ferry).

0022-3115/$ - see front matter © 2010 Elsevier B.V. All rights reserved.
doi:10.1016/j.jnucmat.2010.09.034

Table 1
Mean concentration of He in grains of spent UO_2 fuel (from CESAR5 code).

Time (years)	UO_2 (52 GWd t^{-1})		UO_2 (60 GWd t^{-1})	
	at cm^{-3} [a]	at.%	at cm^{-3} [a]	at.%
300	4.2×10^{19}	0.06	5.0×10^{19}	0.07
1000	7.0×10^{19}	0.1	8.0×10^{19}	0.11
5000	1.2×10^{20}	0.16	1.3×10^{20}	0.18
10,000	1.5×10^{20}	0.21	1.7×10^{20}	0.24
50,000	2.6×10^{20}	0.37	2.8×10^{20}	0.40

[a] Calculated with a grain density of 10.5 g cm^{-3}.

precipitation. This phenomenon had not been observed at a concentration of 0.2 at.% [6].

With these observations, it is difficult to estimate the stability of the spent fuel matrix versus the quantity of He produced by α-decays. Indeed, in these experiments, He is implanted at the sample surface (the depth of implantation is lower than the grain size of 10 μm), which includes grains and grain boundaries. It is not possible to discern He behaviour in the grains from that in the grain boundaries. Furthermore, these data can not evidence the role of fission gas bubbles that are present in the UO_2 pellets after irradiation.

The behaviour of He produced by α-decays in $(U_{0.9}, {}^{238}Pu_{0.1})O_2$ pellet was also investigated by Ronchi and Hiernaut [7]. He concentrations were between 1.9 and 3.8×10^{19} He at cm^{-3} and the cumulative α-damage was about 0.7 displacement per atom (dpa). Transmission Electronic Microscopy (TEM) revealed a population of nanometric He bubbles in the grains and initiation of 10–100 nm micro-cracks. On the other hand, ruptures of grain boundaries in $^{238}PuO_2$ pellets stored for 25 years, where the He content was about 4.7×10^{21} at cm^{-3}, were reported by Roudil et al. [8]. In this case, the cumulative α-damage is very high (~100 dpa), compared to the damage reached in spent UO_2 fuel after 10,000 years of disposal (~2 dpa). Furthermore, the analogy of mechanical properties between PuO_2 and UO_2 pellet needs to be verified.

Other data refers to He behaviour in uraninites, considered as natural analogues of SNF [9]. In those samples, the residual quantity of He was less than 5% of the total production (8.125×10^{20} He/g_{UO2+x}, estimated from the age of deposit). The damage level due to α-disintegrations was also very high (around 180 dpa). TEM evidenced the presence of nanometric bubbles, up to 10 nm in clusters. No micro-cracks were observed in the samples before thermal treatment. In those samples, the high release of He may be due to bubble coalescence and percolation, without creating any other damage in the material. In other respects, the small size of the grains in those samples may have favoured the high release of He.

From these observations, it is actually difficult to draw conclusions about the stability of SNF pellets with an accumulation of He and α-damage. A complementary approach is proposed here. It is firstly based on the analogy between mechanisms of fission gas release in the fuel rod in reactor and the mechanisms of He release in the SNF after placement in a repository. The effects of He on the SNF microstructure are then evaluated by using a simplified model of evolution. It is a first approach to modelling of SNF integrity during long-term storage. It is currently improved to remove part of the large conservatisms that are described in the following.

2. He fate in a spent nuclear fuel rod

The properties of fission gases in nuclear fuel have been intensively investigated due to their impact on the thermo-mechanical behaviour of nuclear fuel rods in reactor. Indeed, a large release of fission gas would increase the internal pressure of the fuel rod and diminish the thermal conductivity of the gap, resulting in a temperature rise of the nuclear fuel. Some models of fission gas release have been proposed in the literature. Their transposition to helium release in spent fuel during disposal is based on the comparison between the conditions of irradiation in reactor and the conditions of repository.

2.1. Mechanisms of fission gas release in the fuel rod during irradiation in reactor

Because of their low solubility in UO_2, the fission gases (Xe and Kr) tend to coalesce as bubbles within the fuel grains above a given concentration. The bubbles range in size between 2 and 100 nm [10]. However, the gas nanobubbles are continuously totally or partially destroyed by fission fragments [11]. During irradiation, a fraction of the gas is thus returned to solution in the matrix, preventing the gas bubbles from acting as ideal sinks. The gas is thus transported to the grain boundaries by simple atomic diffusion and mobility of the gas bubbles at high temperatures.

At grain boundaries, when fission gases reach a sufficient concentration and the local temperature exceeds 800 °C, they can form intergranular bubbles ranging in size from about 0.1 to 1 μm. When the grain boundaries contain a large quantity of gas and the temperature is high enough, the intergranular bubbles coalesce, forming interconnected channels that allow the gas to migrate towards the free volumes of the rod [10]. Gas release by percolation is controlled by the difference between the gas pressure in the pores and in the free volumes and by the fuel permeability. These mechanisms have been evidenced at temperatures above 1300–1400 °C, which are reached during power transients. In normal operation, however, the mechanisms of fission gas release are not so well known.

From [12], the density and size of intragranular bubbles in UO_2 fuel of light water reactor slightly depend on fuel burnup. In general, the diameter lies between 1 and 10 nm, and the density is around 10^{17} bubbles cm^{-3}. The bubble size slightly increases, while the density decreases, with temperature and burnup. For burnup larger than 40 GWd t^{-1} or for high temperatures (e.g. 1200 °C), a second population of bubbles appears. The diameters lie between 20 and 100 nm for a density of 10^{15} cm^{-3}. From [10] the density of intragranular bubbles is correlated to the diameter of the bubble according to:

$$\log_{10}(C_{bieq}) = -2.6 \cdot \log_{10}(d_b) + 25.1 \quad (1)$$

where C_{bieq} is the density of bubbles (bubbles m^{-3}) and d_b is the diameter of bubbles (nm).

At the end of irradiation, the pressure of fission gas bubbles is very high. Nogita and Une [13] have measured by TEM–EDX a density of Xenon ranging between 4 and 6 g cm^{-3} in bubbles of 4 to 10 nm located in grains of the intermediate zone ($0.75 \times R_o$ to $0.95 \times R_o$, with R_o the pellet radius). These values are close to the density of solid Xe. According to the equation of state of gas proposed in [14], these values of density lead to pressures between 1 and 15 GPa at 427 °C, which are two to three times higher than the pressure at equilibrium with the solid. These values are consistent with the observations of [15], which lead to a pressure of 1 GPa at 1000 °C in larger bubbles (50–80 nm), e.g. three times higher than the equilibrium pressure. This overpressure is consistent with a mechanism of bubble growth by dislocation punching [15]. The overpressure occurs when the flow of vacancies into the bubbles is not sufficient to compensate the volume occupied by a gas atom, particularly in a large bubble. This mechanism is more probable at low temperature, at which the diffusion is athermal.

2.2. Mechanisms of He release in a spent fuel rod in a repository

He is created in SNF grains by α-decays of actinides (cf. Table 1). In repository conditions, the mobility of He in the grains of SNF is governed by thermal diffusion on the one hand, and by α-self irradiation enhanced diffusion on the other hand. The processes of diffusion are very limited. At the expected temperatures of geological disposal, from 200 °C to about 100 °C before arrival of water in the container, the pure thermal diffusion of He is not significant, even for the long-term [16]. Furthermore, the upper estimate of the diffusion coefficient enhanced by α self-irradiation proposed in [17] decreases with time, from around 10^{-25} to 10^{-26} m^2 s^{-1} over 10,000 years in a UO_2 fuel of 47.5 GWd t^{-1}. If we consider these values for He diffusion, the diffusion length of helium atoms is about 0.15 μm after 10,000 years of disposal.

Some authors have observed an acceleration of thermal diffusion with cumulative α-damage. In a sample with a α-damage of 0.3 dpa, the diffusion coefficient of He was five times higher than the diffusion coefficient in pure UO_2 [18]. The diffusion studies performed on (U, Pu)O_2 pellets with a cumulative α-damage of 0.7 dpa led to a thermal diffusion, which is one hundred times higher [7]. This same value was measured on PuO_2 samples with very high α-damage (100 dpa) [19]. This observation indicates a rapid saturation of the acceleration of thermal diffusion due to α-damage from a very low level of damage. The maximal value of the thermal diffusion coefficient is lower than 10^{-26} m^2 s^{-1} for the temperatures lower than 200 °C. Consequently, the enhancement of thermal diffusion by α-damage is of second order compared to diffusion enhanced by α self-irradiation.

On the other hand, the solubility of He in UO_2 is very low [20]. The solubility should increase with irradiation defects, pores and grain boundaries but the solubility value in SNF is difficult to determine. If we consider the value measured in polycrystalline UO_2, a pressure of 50 bar at 25 °C in the spent fuel rod at the end of irradiation, and a temperature between 20 and 200 °C, the solubility range of He is from 0.01 to 0.02 at.%. Such concentrations of He are reached after some decades of repository in spent UO_2 fuel (cf. Table 1). The conditions of nuclear fuel irradiation are compared with the conditions of SNF in a repository in Table 2.

Due to the low solubility and low mobility of He atoms under repository conditions, He should accumulate in SNF grains, and form bubbles, which are stable as soon as:

$$P_b \geqslant P_{hyd} + \frac{2\gamma}{r_b} \quad (2)$$

where P_b is the pressure in the bubble, γ is the UO_2 free surface energy (J m^{-2}) and P_{hyd} is the external pressure.

The preferential sites for the nucleation of He bubbles should be the defects created by irradiation in reactor, or by α self-irradiation in disposal. If the length of diffusion of He atoms is large compared to the distance between two fission gas bubbles of SNF grains, He atoms could be trapped in the fission gas bubbles. Hence, due to He accumulation, the initial characteristics of the bubble population (size, density and pressure) should evolve during disposal.

A model of He evolution in grains of SNF may be derived from the models of fission gas release, by taking into account the properties of He instead of Xe in UO_2, and the conditions of temperature and irradiation of disposal. Such a model would require calculating the concentration of He atoms dissolved in the UO_2 grains, the quantity of He atoms forming new bubbles or being trapped in the fission gas bubbles, as well as the characteristics of these bubbles. It would be necessary to evaluate the relevance of the mechanisms of migration under disposal conditions, and the parameters of migration that are too low to be measured by Lab-experiments at the temperature of interest.

He atoms are released into grain boundaries by diffusion in the grain (no bubble migration at the temperature of concern). The released fraction of He after 10,000 years should be very limited since the diffusion length is lower by one to two orders of magnitude than the size of the grains. If the accumulation of He in the grains leads to the rupture of the material, then He atoms will be released into grain boundaries. Different scenarios lead to He release into the free volume of the SNF rod: (i) diffusion along the grain boundaries, (ii) opening of the grain boundaries if the critical stress is exceeded due to He accumulation, or (iii) percolation if the coverage of grain boundaries by bubbles is sufficient (∼0.5), allowing the interlinkage of bubbles along grain boundaries.

2.3. Consequences of helium on the microstructure of spent fuel pellet

The fate of He in the spent fuel pellet depends not only on He diffusion and solubility in UO_2 but also on the mechanical and morphological characteristics of the spent fuel microstructure after irradiation.

As fabricated, the fuel pellet consists of UO_2 grains of about 10 μm. After irradiation, two main regions appear in the UO_2 fuel pellet with a mean burnup higher than 40 GWd t^{-1}:

- The central and intermediate zones (0–0.96 × R_o), where the grains have the same size as before irradiation. In the central zone (0–0.5 × R_o), small intragranular bubbles precipitate and micrometer size bubbles appear in the grain boundaries. In the intermediate zone, some nanometric bubbles in grain boundaries are revealed by chemical etching. Vickers micro-indentations evidence that this zone corresponds to the maximal embrittlement of grain boundaries [23].
- At the periphery of the pellet (0.96 × R_o to R_o), the microstructure is deeply modified both by the appearance of large pores and by subdivision of the grains. The fully restructured zone (*optical rim*), with a thickness from 75 to 140 μm, is highly porous (15%). The sizes of the polyhedral and rounded subgrains are around 0.5 μm and 0.1–0.2 μm, respectively. The mean diameter of the gas bubbles located in the grain boundaries is

Table 2
Comparison between in reactor and repository conditions.

In-reactor conditions	Repository conditions
Short irradiation time (5–6 years) and high temperature (400 to 1200 °C) High production rate of fission gases, typically 3×10^{18} at m^{-3} s^{-1}	Long-time before water arrival (10,000 years) and low temperature (<200 °C) Low production rate of He: $\leqslant 9 \times 10^{15}$ at m^{-3} s^{-1} in a UO_2 fuel of 60 GWd t^{-1}
Physico-chemical properties of fission gases in UO_2 Mean diffusion length during irradiation ≈5 μm	*Physico-chemical properties of He in UO_2* Small distance of diffusion ≈0.15 μm after 10,000 years
Maximal solubility = 3×10^{-10} at.Xe/at.U/atm	Solubility range: Mono-crystalline UO_2: 2.7×10^{-7} at.He/at.U/atm [21] Poly-crystalline UO_2: 7.5×10^{-6} at.He/at.U/atm [22]
Damages created by fission reactions More or less ductile material	Damages due to α self-irradiation (recoil atom + α particle) Brittle material

1 μm. The local burnup is two to three times higher than the mean pellet burnup. The rim zone, which corresponds to the loss of Xe detection by microprobe, includes also a transition zone, which contains pristine grains and subgrains. The thickness of this zone increases with the mean local burnup [24].

Everywhere else but the rim, we expect that the most part of He remains in the grain due to the low value of the diffusion length. Considering the low value of solubility and the production rate of He in UO_2 spent fuel, He should precipitate in the grain, eventually forming new He bubbles, or being trapped in pre-existing fission gas bubbles. These two scenarios and their consequences will be discussed in the next part.

In the rim region, the grains are so small that a large part of the created He could be released into the large pores located at the grain boundaries, which are already over-pressurized by fission gases. The consequences of He accumulation in the large pores will be assessed.

The assumptions and uncertainties of the theoretical approaches proposed in the next parts will be discussed in part 5.

3. Evolution of the pristine grains of spent nuclear fuel during repository

A complete model of He transport in SNF would lead to large uncertainties regarding the parameters of the model at the temperature of concern. We propose here a simplified approach in order to estimate the effect of He on the stability of large grains of the SNF pellet. This simplified approach is based on conservative assumptions regarding the mechanisms involved in He migration.

The thermal diffusion of He is higher by some orders of magnitude than the thermal diffusion of uranium and fission gas [25], and the flux of He atoms in bubbles should be larger than the flux of U vacancies. The most conservative scenario is thus considered: the transport of He atoms into bubbles without any vacancy. In this case, the flux of He atoms into the bubbles leads to a pressurization of bubbles, as observed for fission gas bubbles during irradiation. Furthermore, we consider that the efficiency of He atom trapping by bubbles is not reduced by the increase of pressure in the bubbles. At the repository temperature, the dissolution and migration of bubbles are not relevant even after a long time. Due to its low efficiency, the dissolution of bubbles by α self-irradiation is neglected [26]. The thermal and athermal diffusion of U atoms are extremely low under repository conditions (respectively $<10^{-30}$ m^2 s^{-1} from [25] and $<10^{-28}$ m^2 s^{-1} from [17]). Therefore, the deformation by creep around the bubbles is neglected for the period of concern (10,000 years). In summary, all the phenomenon that could lead to the growth of bubbles with incoming flux of He atoms are not taken into account in the model. Hence, the trapping of He atoms can lead to large pressures in the bubbles without modifying the size of the bubbles.

In the pristine matrix of the pellet, He atoms can form new bubbles in the grains or/and can be trapped in the pre-existing fission gas bubbles. The probability of trapping by fission gas bubbles depends on the distance between two bubbles and on the diffusion length of He atoms during 10,000 years. Each scenario is independently treated afterwards. The evolution of the pressure in the bubbles is calculated with the following assumptions:

- The bubbles are spheres of the same size, uniformly distributed in the grain.
- The gas in the bubble is at thermodynamic equilibrium. The pressure of the gas is linked to the volume and temperature of the gas by an appropriate equation of state of gas.

The calculations are made for various populations of bubbles and each population is characterized by the diameter and the density of bubbles.

3.1. The equations of state of gas

When the gas density in the bubble is low, the equation of state of perfect gas allows linking the gas pressure in the bubble and the volume of gas atom

$$P_b = \frac{k \cdot T}{V_{at}} \tag{3}$$

where P_b is the bubble pressure (Pa), V_{at} is the volume of gas atom (m^3), T is the temperature of the gas (K) and k *is* the Boltzmann's constant (1.38×10^{-23} J K^{-1}).

However, at the end of irradiation, the density of gas in bubbles is very high, close to the density of solid Xenon. The equation of state of Xenon is chosen as a function of the gas density, according to Muller-Casanova's recommendations [27]. These equations are also those used in the model of fission gas behaviour in nuclear fuel, MARGARET [28]:

- The complete equation of van der Waals for Xe is applied for the moderate pressures (e.g. $V_{at} \geqslant 1.6 \times 10^{-28}$ m^3)

$$P_b = \frac{k \cdot T}{V_{at} - B} - \frac{A}{V_{at}^2} \tag{4}$$

  with $B = 86 \times 10^{-30}$ m^3 and $A = 1.16 \times 10^{-48}$ Pa m^{-6} [29].
- For higher gas pressure, corresponding to $V_{at} \leqslant 1 \times 10^{-28}$ m^3, the equation of Carnahan–Starling with the modified potential of Buckingham is applied.

$$P_b = \frac{kT}{V_{at}} \cdot \frac{1 + y + y^2 - y^3}{(1-y)^3} \tag{5}$$

  with y, the reduced density of gas and d the diameter of hard sphere (m), given respectively by [27]

$$y = \frac{(\pi d^3/6)}{V_{at}} \tag{6}$$

  and

$$d = 4.45 \times 10^{-10}\left(0.8542 - 0.03996 \cdot \ln\left(\frac{T}{231.2}\right)\right) \tag{7}$$

Moreover, the minimal value of the atom gas volume for Xe is 3.14×10^{-29} m^3 [14]. It yields a maximal pressure of 78 GPa at 200 °C.

For intermediate values of V_{at} (1×10^{-28} m$^3 \leqslant V_{at} \leqslant 1.6 \times 10^{-28}$ m^3), a weighted value of these two equations is used to ensure the continuity of pressure calculations over the whole domain of V_{at}. Fig. 1 shows the consistency between the pressures calculated at 200 °C according to Eqs. (4)–(7), and the values tabulated by Ronchi for Xenon at 127 °C and 227 °C in [14]. The equations of state of Xenon are used to calculate the pressure in bubbles of fission gases and, conservatively, in bubbles containing fission gases plus He.

As for bubbles containing only helium, the equation of Carnahan–Starling (Eq. (5)) is used, with the reduced density of gas given by [30]: $y = \frac{B}{4V_{at}}$, with B the co-volume for Helium (3.95×10^{-29} m^3 [29]). This analytical high density equation of state ensures the continuity with the van der Waals equation for Helium (Fig. 2).

The minimum volume considered for Helium gas atom ($V_{\min}$) corresponds to the volume of hard spheres at closest-packing and relates to the co-volume B, by

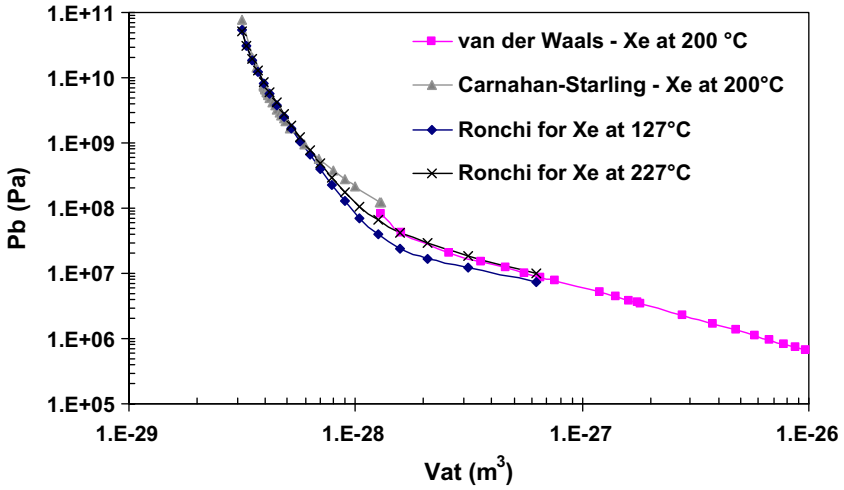

Fig. 1. Comparison of the pressures of Xenon calculated at 200 °C by Carnahan–Starling and van der Waals equations with the data from Ronchi [14].

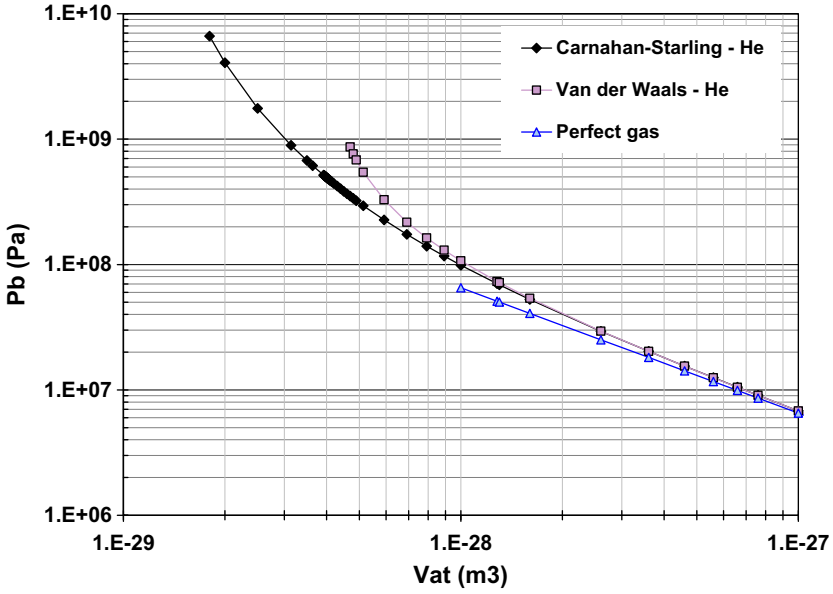

Fig. 2. High density equation of state for Helium (Carnahan–Starling) and comparison with the van der Waals and perfect gas laws, at 200 °C.

$$V_{\min} = \frac{3B}{2\pi\sqrt{2}} = 1.3 \times 10^{-29}\ \mathrm{m}^3$$

This value leads, at 200 °C, to a maximal pressure of 69 GPa. In the above expressions for Helium, the effect of temperature on the diameter of the hard sphere is not taken into account. This analytical equation of state yields higher pressure than the equation of state proposed by Wolfer [31], who takes into account the decrease of the hard sphere diameter with temperature (Fig. 3). The choice of the equation of state for Helium is also conservative compared to experimental values [32], but less conservative than considering Xenon properties for Helium bubbles (Fig. 4).

3.2. Characteristics of fission gas bubbles in spent fuel grains after irradiation

The pressure and size of fission gas bubbles after irradiation are calculated by assuming that the spherical bubbles are at mechanical equilibrium with UO_2 surface. The bubble pressure depends on the bubble radius

$$P_b = P_{hyd} + 2\gamma/r_b \qquad (2)$$

γ is the surface energy in J m^{-2}. γ varies with the temperature [33]:

$$\gamma = 0.85 - 1.4 \times 10^{-4} \times T \qquad pour\ 0 < T < 2850\ ^\circ\mathrm{C}$$

with T the temperature in Celsius degree. This relationships does not take into account the corrective factor $(0.41 \times \gamma)$ recommended by the authors for the calculation of pressure in a cavity; the justification is not clear and a conservative approach has been preferred to calculate the initial pressures of the bubbles. P_{hyd} is the hydrostatic pressure resulting from the cooling water and the cladding stress, assuming that the internal stresses are relaxed at the temperature of irradiation (P_{hyd} = 16 MPa).

The equation of state of gas allows calculation of the volume of gas atoms in the bubble, and, from the volume of the bubble, deducing the total quantity of gas atoms in the bubble. The pressure and corresponding quantity of gas atoms in the bubbles are given in Table 3 for various populations of bubbles. The size and density that are taken into account in these calculations are consis-

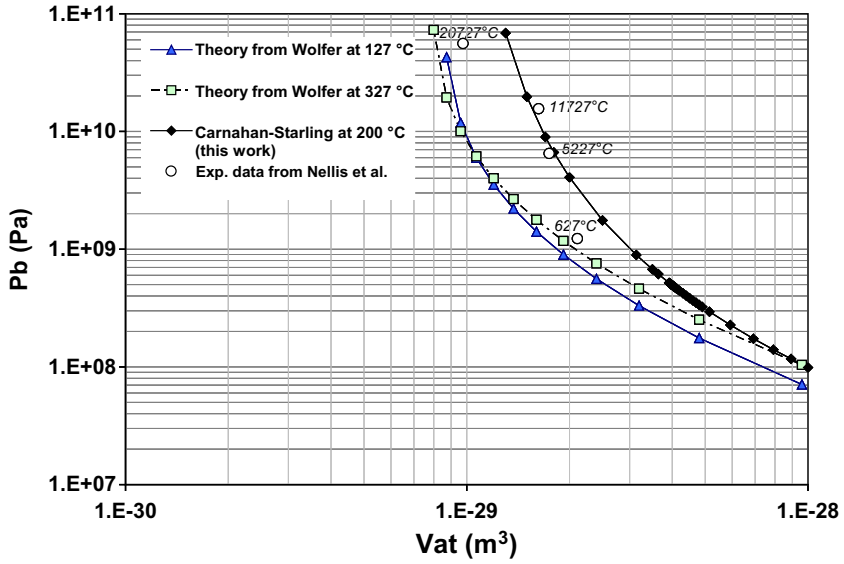

Fig. 3. Comparison of the equation of state for Helium at 200 °C (this work) with the theory of Wolfer (from Table 1 in [31]) and experimental data from [32]; the temperatures in italics correspond to the interpretation of experimental data [32].

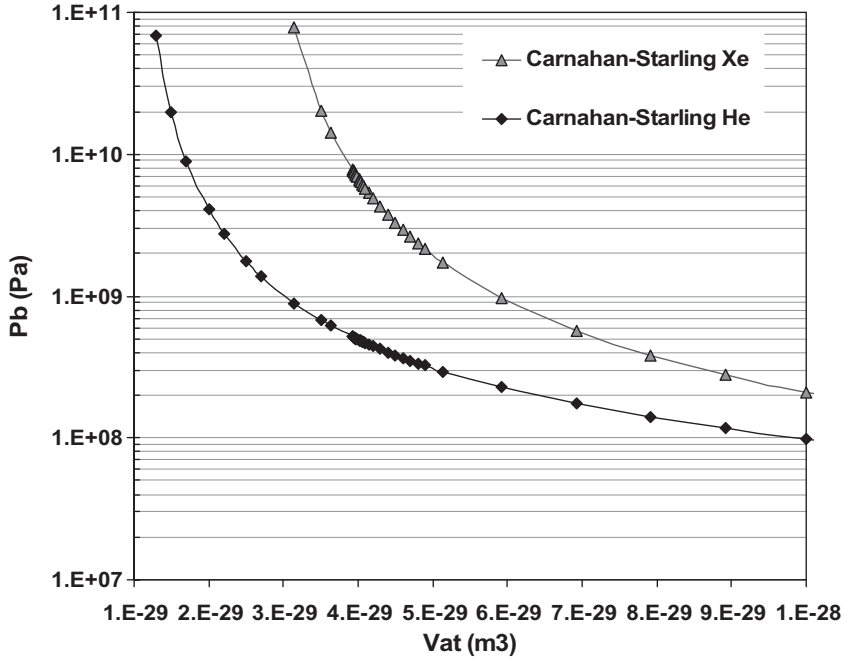

Fig. 4. Comparison of Carnahan–Starling equations for Xe and He at 200 °C.

tent with the bubble populations observed in grains of UO_2 fuels at the end of irradiation. We also note that the mean distance between two bubbles is lower than the upper estimate of the diffusion length of He in SNF after 10,000 years.

3.3. Pressure increase in the fission gas bubbles due to He

The mechanisms of bubble dissolution or bubble growth are not effective at low temperature. Thus, during in-pool storage of SNF, the size and the number of bubbles do not evolve, despite the change of external temperature and pressure.

Over the long-term, the bubble size is fixed as a model assumption. The flux of He atoms into the fission gas bubbles will contribute to the pressure increase in the bubble. The total pressure after 10,000 years of disposal due to He and fission gases is calculated by considering that all He atoms produced by α-decays will be trapped in the bubbles. For each population of bubbles, we deduce the total quantity of gas atoms in the bubble, the corresponding volume of gas atoms, and with the appropriate equation of state, the pressure in the bubble at 200 °C, the maximal expected temperature of the repository (Table 4).

The assumption that all He atoms can be indefinitely trapped in bubbles of 2 nm, without any increase of the bubble size, leads to volumes of gas atom, which are lower than the minimal volume. Therefore the maximal pressure (78 GPa) should be reached before 10,000 years in the 2 nm bubbles. For the bubbles with a size be-

Table 3
Pressure (P_b^{eq}), volume of gas atom (V_{at}) and quantity of gas atoms (n_{at}) in the bubble at equilibrium in UO_2 at the end of irradiation (T = 400 °C, P_{hyd} = 16 MPa), for each population of bubbles.

Diameter d_b (nm)	2	10	50	100
Density (number of bubbles m^{-3})	10^{23}	5×10^{22}	5×10^{20}	10^{20}
Grain porosity, w (%)	0.04	2.6	3.3	5
Mean distance between the surface of bubbles (m)	1.9×10^{-8}	1.7×10^{-8}	7.6×10^{-7}	1.1×10^{-7}
P_b^{eq} (MPa)	1604	334	80	48
V_{at} ($\times 10^{-29}$ m^3)	5.47	9.27	16	21.1
n_{at} (at/bubble)	77	5648	4.09×10^5	2.48×10^6

Table 4
Quantity of gas atoms (n_{at}), volume of gas atom (V_{at}) and pressure (P_b) at 200 °C in the bubble due to He accumulation in the fission gas bubbles, for a UO_2 fuel of 60 GWd t^{-1} after 10,000 years of disposal.

Diameter d_b (nm)	2	10	50	100
Density of bubbles (number of bubbles m^{-3})	10^{23}	5×10^{22}	5×10^{20}	10^{20}
n_{at} (at/bubble)	1.8×10^3	9.0×10^3	7.5×10^5	4.2×10^6
V_{at} (10^{-29} m^3)	$\ll V_{min}$	5.79	8.74	12.5
P_b (MPa)	P_{max}*	1048	292	130

* The maximal pressure (78 GPa) is reached before 10,000 years.

tween 10 and 100 nm, the pressure, derived from the Carnahan–Starling equation of Xenon, varies roughly between 1 and 0.1 GPa.

3.4. Characteristics of new He bubbles

If the density of fission gas bubbles in the grains is low compared to the potential mobility of He atoms in SNF, He should form new bubbles with a size ranging from 1 to 100 nm, as soon as the limit of solubility is reached. The second scenario to evaluate is thus the formation of new bubbles in the grains.

The density of He bubbles created by He accumulation in the grain is a priori not known. This parameter is considered as a variable depending on the bubble size and obeys to the following criteria:

- Considering that all He atoms produced by α-decays in the grain can reach a bubble, the mean distance between two bubbles must be lower than two times the diffusion length of He atoms (<0.3 μm).
- The volume of a gas atom in the bubble must be higher than the minimal volume of gaseous He (1.3×10^{-29} m^3).
- The condition for bubble stability, e.g. $P_b \geqslant P_{hyd} + 2\gamma/r_b$, in repository conditions (T = 200 °C and P_{hyd} = 0, considering the absence of external stress on the pellet) is achieved.
- The distance between two bubbles must be higher than the coalescence threshold (6×10^{-9} m, from [10]).

The quantity of He atoms per bubble is calculated as a function of the size and density of the bubbles assuming that all He atoms are trapped in bubbles. The equation of Carnahan–Starling of He allows calculation of the pressures in the bubbles. For a given size of the bubble, the range of possible densities is selected according to the above criteria. The values of the corresponding porosity and pressure are reported in Table 5. For this scenario, we consider that the density of fission gas bubbles is not sufficient to trap He atoms. The porosity of the grain corresponds thus to the volume of He bubbles. Assuming that all He atoms will precipitate in He bubbles, the maximal pressure (69 GPa) could be reached in bubbles lower than 50 nm for the low values of bubble density.

3.5. Rupture criterion

The value of the critical pressure, which should lead to the development of micro-cracks in a material consisting of UO_2 solid and homogeneous gas bubbles uniformly distributed in UO_2 has been proposed in [34]. By writing the condition of equilibrium of the internal stresses in the material, without external stress, the authors link the critical value of the bubble pressure with the tensile fracture stress measured on the solid, and the material porosity

$$p_b^{fail} = \sigma_{fail} \cdot \frac{1 - (2/3) \cdot w + (1/9) \cdot w^2}{(2/3) \cdot w - (1/9) \cdot w^2} \quad (8)$$

where p_b^{fail} is the critical pressure (Pa), σ_{fail} is the fracture stress (Pa) and w is the material porosity (–).

The critical pressure of the bubbles is represented in Fig. 5 as a function of the material porosity. The value of the fracture stress (150 MPa) is derived from mechanical tests performed on unirradiated UO_2 pellets [35].

From the simplified approach proposed in the paragraphs above, we have calculated the pressure in the bubbles of the grains after 10,000 years of disposal, according to two scenarios: the trapping of all He atoms in the fission gas bubbles or the formation of new He bubbles. With the very conservative assumptions of the model, which is based on mass balance, the maximal pressure (78 GPa) could be reached before 10,000 years in fission gas bubbles of a few nanometers (*see* Table 4). Anyhow, such a population of bubbles leads to a very low porosity and very high critical values of the bubble pressure. Hence, whatever the population of fission gas bubbles, the pressure of the bubbles remains lower by one order of magnitude, at least, than the critical values of pressure.

Actually, the population of fission gas bubbles is not homogeneous in the grain. The diffusion of He atoms in the solid will be governed by the gradient of physico-chemical potential: the efficiency of trapping by bubbles should decrease when the bubble pressure will increase. Thus, it is more probable that He atoms will migrate into the large bubbles, where the pressure is lower [36]. In spite of the conservative assumption that all He atoms are trapped in fission gas bubbles, whose size is fixed, the pressures in the bubbles are relatively low compared to the critical values. Therefore, the overpressure of the fission gas bubbles, caused by He production during 10,000 years, should not lead to the microcracking of the SNF grains.

In the case of formation of new He bubbles, if we consider that all He atoms precipitate in bubbles, the lowest densities of bubbles lead to very high pressure (69 GPa). However in this case, the grain

Table 5
Variation range of the characteristics of new He bubbles in grains of a UO_2 fuel of 60 GWd t^{-1}, at 200 °C and after 10,000 years of disposal, depending on the size of the He bubble.

Diameter d_b (nm)	2	10	50	100
Density of bubbles (number of bubbles m^{-3})	5.4×10^{23}–1×10^{24}	4.3×10^{21}–1.5×10^{22}	3.4×10^{19}–3×10^{20}	2×10^{19}–7×10^{19}
Porosity due to He bubbles, w (%)	0.2–0.4	0.2–0.8	0.2–2	1–3.6
Mean distance between bubble surfaces (m)	(10–8) $\times 10^{-9}$	(5–3) $\times 10^{-8}$	(2.6–1.0) $\times 10^{-7}$	(2.6–1.4) $\times 10^{-7}$
P_b (MPa)	54,000–1844	56,500–360	63,800–80	212–37

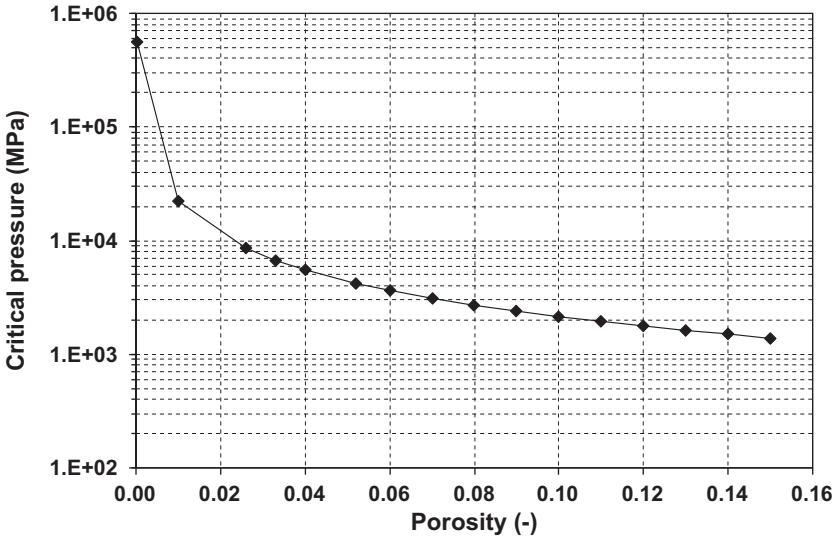

Fig. 5. Critical bubble pressure as a function of the total porosity of the UO_2 grains, considering that the population of bubbles is homogeneous.

porosity is also so low that, whatever the bubble size and density, the bubble pressure remains lower than the critical pressure. For example, in the bubble of 2 nm, the pressure is lower than the critical pressure, by a factor of two for the lowest density and by a factor of 30 for the highest density. If we consider for this scenario also the presence of some fission gas bubbles, the porosity of the grain will increase and the critical bubble pressure decrease. However, with the increase of the total number of bubbles that are able to trap helium, the pressure per bubble will also decrease.

This second scenario is also very conservative. It would be necessary to improve this approach by taking into account the processes of He transport, of bubble nucleation and bubble growth in order to calculate the bubble populations, which could be formed under disposal conditions. Furthermore, the maximal distance of diffusion of He atoms during 10,000 years (0.3 μm) is based on an upper estimate of the athermal diffusion coefficient. This maximal diffusion length constrains the minimal value of the bubble density. If we demonstrate that the diffusion of He is lower, the bubble density to consider in the calculations will be higher. Consequently, the quantity of He atoms per bubble will decrease, and the pressure in the bubbles as well. Again, we can conclude that microcracking of the grains by He bubble formation is not expected.

4. Evolution of the rim pores

4.1. Evolution of the pressure in the pores of the rim

In the fully restructured zone, we consider that the most part of He atoms will be released by diffusion into the pores located at the grain boundaries. These pores already contain the fission gases at the end of irradiation. The pressure in the pores at the end of irradiation is calculated versus the size of the pores, according to the same approach as described previously in Section 3.2.

Table 6
Pressure (P_b^{eq}), volume of gas atom (V_{at}) and number of gas atoms (n_{at}) in the pores of the rim, at equilibrium at the end of irradiation (T = 400 °C, P_{hyd} = 16 MPa) for each population of pores.

Diameter (μm)	0.5	1	2	2.5
Density (number of pores/m^3)	2.3×10^{18}	2.8×10^{17}	3.6×10^{16}	1.8×10^{16}
Mean distance between pore surfaces (m)	2.6×10^{-7}	5.1×10^{-7}	1.0×10^{-6}	1.3×10^{-6}
P_b^{eq} (MPa)	22	19	18	17
V_{at} (10^{-28} m^3)	4	4.8	4.9	5.2
n_{at} (at/pore)	1.64×10^8	1.09×10^9	8.55×10^9	1.57×10^{10}

Table 7
Quantity of gas atoms (n_{at}), volume of gas atom (V_{at}) and pressure (P_b) at 200 °C in the pores of the rim due to He accumulation in the pores, for a UO_2 fuel of 60 GWd t^{-1} after 10,000 years of disposal.

Pore size (μm)	0.5	1	2	2.5
Density (number of pores/m^3)	2.3×10^{18}	2.8×10^{17}	3.6×10^{16}	1.8×10^{16}
n_{at} (at/pore)	3.5×10^8	2.6×10^9	2.0×10^{10}	3.9×10^{10}
V_{at} (10^{-29} m^3)	19	20	21	21
P_b (MPa)	31	28	26	26

The value of the pore density is chosen as a function of the pore size, so that the total porosity of the zone is 15%. The mean distance between the pore surfaces is consistent with the values of Spino et al. [37]. The pressure at equilibrium at the end of irradiation (at 400 °C) and the corresponding quantity of gas atoms are reported in Table 6 as a function of the pore size. If we consider the over-pressurization of fission gas bubbles observed in the rim zone after irradiation, the quantity of gas atoms in the pores would be two to three times larger than the values given in Table 6.

The pressures are calculated by considering that all He atoms locally produced during 10,000 years will be trapped in the pores (Table 7). For these calculations, we assume that the local concentration of He is 2.5 times larger than the mean quantity of He in the pellet. Due to the large size of the pores in the restructured zone, the pressure remains low.

If we take into account an initial quantity of fission gas in the pore, which is two times the quantity expected at equilibrium, the calculated pressures are about two times higher than the values of Table 7.

4.2. Rupture criterion for the rim region

The determination of the critical pore pressure which would lead to the propagation of cracks in the rim zone is based on the theory of rupture of polycrystalline ceramics. In the restructured zone of the pellet, the pores of large size constitute flaws at the grain boundaries, from which fracture can initiate [35]. The

strength of brittle ceramics at low temperature is based on the Griffith's law, which links the stress intensity factor with the size of the initial flaw [38]:

$$K_I = A \times \sigma \times c^{1/2} \quad (9)$$

where K_I is the stress intensity factor (MPa $m^{1/2}$), σ is the applied tensile stress (MPa), and c is a characteristic dimension of the flaw (m). A is a constant, which depends on the crack geometry and the type of the loading. The most critical flaw in ceramics corresponds to a value of $\pi^{1/2}$ for A.

The flaw propagates spontaneously to failure as soon as the stress intensity factor reaches a critical value, K_{IC} (MPa $m^{1/2}$), which corresponds to the material toughness.

An indication of the fracture toughness of the rim material can be inferred from the Vickers indentation tests [37]. Matzke and Spino [39] evidences an increase of the strength to fracture in the rim zone with a value of K_{IC}, which is higher by a factor of two compared to unirradiated UO_2 and the rest of the pellet. For the authors, the improvement of the material strength is due to the refinement of the grains, overwhelming the detrimental effect of pores generally observed in ceramics. In the fully restructured zone, the fracture toughness lies between 2 and 3 MPa $m^{1/2}$.

If we assume that the pores constitute the limiting defects of the rim, the critical pressure depends on the size of the pores. The value of the critical pressure decreases from 1600 MPa for the pores of 0.5 μm to 700 MPa for the pores of 2.5 μm.

It appears from Table 7 that, whatever the pore size, the pressure of the pores is 10–50 times lower than the critical pressure. In conclusion, the conditions of crack propagation, due to the release of all He atoms in the pressurized pores, should not be reached in the rim region.

5. Discussion

The uncertainties regarding the proposed model of spent fuel evolution concern the pressure estimates and the rupture criteria. As for the evolution of the gas pressures in the bubbles, the calculations are based on the choice of the equations of state of gas. This choice is consistent with other literature data, but remains difficult to validate. The main uncertainties are bounded to the rupture criteria. In order to ensure the conservatism of the approach, the model is based on conservative assumptions, which yield very high values of pressure in the gas bubbles, as summarized below:

- We consider that all He atoms will be trapped in bubbles, whereas a part of the He should be dissolved in the UO_2 matrix; He solubility in SNF is not well known. With the upper values between 0.1 and 0.3 at.%, as suggested by Roudil et al. [3], the dissolved fraction could represent 50–100% of the He inventory after 10,000 years in a spent UO_2 fuel.
- The population of bubbles in the grains is assumed as homogeneous in size and the efficiency of the trapping by bubbles is the same, whatever the pressure in the bubble. In reality, the size of the bubbles in the grain is not uniform and He atoms should preferentially diffuse to the large bubbles, where the pressure is relatively low.
- Trapping by bubbles is considered as infinite leading to very high overpressures in the small bubbles. Such high pressures could, in the long-term, produce deformation of the material by creep even at the low temperature of disposal, leading to bubble growth and the diminishing of pressure. At high density of gas, a relative increase of volume of 1% will lead to a relative decrease of pressure of more than 4%. The bubble swelling was neglected here, leading to a very high overestimation of the pressure in the 2 nm bubbles. For that population of bubbles, if we consider a small initial overpressure of 3% compared to the equilibrium pressure and an athermal diffusion coefficient of 9×10^{-30} m^2 s^{-1} for U atoms (from Eq. (19) in [17]), the increase of the bubble volume due to the flux of vacancies would be about 2% after one hundred years, and the equilibrium pressure should be reached. However, this rough estimate takes into account neither the slowdown of creep with time, due to the decrease of the bubble pressure when the volume of the bubble increases, nor the flux of new Helium atoms in the bubble. In order to have a realistic estimate of bubble pressure, it would be necessary to take into account the variation with time of He production, He atoms diffusion, and flux of vacancies in the bubble, and, also the coupling between these processes.

Finally, the pressures in the bubbles have been calculated for a temperature of 200 °C. The temperature of spent fuel packages will depend on the design of the disposal. This maximal temperature has been chosen in order to be not too restricted regarding the concept of the repository and, also, in order to ensure that the conclusions can be applied in the case of a dry storage of shorter duration. The present design of a deep geological repository would lead to a temperature that is close to 40 °C after 10,000 years, and a value of pressure in large bubbles, which is lower by about a factor 1.5 than the values at 200 °C. However, at high density of gas, such as in small bubbles, the temperature has almost no effect on pressure.

In spite of the conservative assumptions of the model, the trapping of all He atoms in fission gas bubbles or the formation of new He bubbles yield values of bubble pressure or pore pressure which are much lower than the critical values derived from the rupture criteria. Therefore, the rupture of the large grains and the propagation of cracks in the rim zone are very unlikely in spent UO_2 fuel during the first 10,000 years of repository.

Finally, the results of the model are consistent with the observations of Guilbert et al. (cf. Section 1), who observed a flaking effect in UO_2 implanted with He at a concentration of 1.1 at.%, due to the bubble formation during thermal treatment. This phenomenon does not appear at a concentration of He of 0.2 at.%, which is close to the concentration of He in spent UO_2 fuel after 10,000 years of disposal.

We can conclude that the pellet microstructure should not evolve before the breaching of the canister. Consequently, the Instant Release Fraction can be considered as the radionuclide inventories located in the free volumes of the SNF rod after irradiation. The IRF values can thus be derived from the leaching tests on spent fuel fragments. The uncertainties of IRF values will strongly depend on the available leaching data, versus the spent fuel burnup and linear power rating.

Acknowledgments

This work is performed in the framework of the research program PRECCI, funded by EDF and CEA. The authors also thank J.M. Gras for his faithful support. Thanks also go to L.H. Johnson and the two anonymous reviewers for their corrections and remarks that have allowed improvement of the paper.

References

[1] L.H. Johnson, C. Ferry, C. Poinssot, P. Lovera, J. Nucl. Mater. 346 (2005) 56–65.
[2] C. Ferry, C. Poinssot, C. Cappelaere, L. Desgranges, C. Jégou, F. Miserque, J.P. Piron, D. Roudil, J.M. Gras, J. Nucl. Mater. 352 (2006) 246–253.
[3] D. Roudil, X. Deschanels, P. Trocellier, C. Jegou, S. Peuget, J.M. Bart, J. Nucl. Mater. 325 (2004) 148–158.
[4] G. Martin, P. Garcia, H. Labrim, T. Sauvage, G. Carlot, P. Desgardin, M.F. Barthe, J.P. Piron, J. Nucl. Mater. 357 (2006) 198–205.
[5] S. Guilbert, T. Sauvage, H. Erralmi, M.F. Barthe, P. Desgardin, G. Blondiaux, C. Corbel, J.P. Piron, J. Nucl. Mater. 321 (2003) 121–128.

[6] S. Guilbert, T. Sauvage, Ph. Garcia, G. Carlot, M.F. Barthe, P. Desgardin, G. Blondiaux, C. Corbel, J.P. Piron, J.M. Gras, J. Nucl. Mater. 327 (2004) 88–96.
[7] C. Ronchi, J.P. Hiernaut, J. Nucl. Mater. 325 (2004) 1–12.
[8] D. Roudil, X. Deschanels, P. Trocellier, C. Jegou, S. Peuget, J.M. Bart, Mat. Res. Sym. Proc. 932 (2006) 529–536.
[9] D. Roudil, J. Bonhoure, R. Pik, M. Cuney, C. Jégou, F. Gauthier-Lafaye, J. Nucl. Mater. 378 (2008) 70–78.
[10] S. Kashibe, K. Une, K. Nogita, J. Nucl. Mater. 206 (1993) 22–34.
[11] H. Blank, Hj. Matzke, Radiat. Eff. 17 (1973) 57–64.
[12] P. Lösonen, J. Nucl. Mater. 280 (2000) 56–72.
[13] K. Nogita, K. Une, Nucl. Instrum. Methods Phys. Res., Sect. A 141 (1998) 481–486.
[14] C. Ronchi, J. Nucl. Mater. 96 (1981) 314–328.
[15] L.E. Thomas, Condensed-phase xenon and krypton in UO_2 spent fuel, in: S.E. Donnely, J.H. Evans (Eds.), Fundamental Aspects of Inert Gases in Solids, Plenum Press, NewYork, 1991, pp. 431–441.
[16] C. Ferry, C. Poinssot, V. Broudic, C. Cappelaere, L. Desgranges, P. Garcia, P. Lovera, P. Marimbeau, J.P. Piron, A. Poulesquen, D. Roudil, J.M. Gras, P. Bouffioux, Synthesis on the Spent Fuel Long Term Evolution, CEA Report, CEA-R-6084, 2005. p. 257.
[17] C. Ferry, P. Lovera, C. Poinssot, P. Garcia, J. Nucl. Mater. 346 (2005) 48–55.
[18] Y. Pipon, C. Raepsaet, D. Roudil, H. Khodja, Nucl. Instrum. Methods Phys. Res., Sect. A 267 (2009) 2250–2254.
[19] Roudil, Pers. Com.
[20] E. Maugeri, T. Wiss, J.P. Hiernaut, K. Desai, C. Thiriet, V.V. Rondinella, J.Y. Colle, R.J.M. Konings, J. Nucl. Mater. 385 (2009) 461–466.
[21] P. Sung, Equilibrium Solubility and Diffusivity of Helium in Single-crystal Uranium dioxide. U.M.I. Dissertation Services, University of Michigan, USA, Ph. D. Chemistry, 1967.
[22] F. Rufeh, D.R. Olander, T.H. Pigford, Nucl. Sci. Eng. 23 (1965) 335–338.
[23] NF-PRO EU Project (contract number: FI6W-CT-2003-02389). Final synthesis report: RTD Component 1. Dissolution and release from the waste matrix, 2008.
[24] Y.H. Koo, B.H. Lee, J.S. Cheon, D.S. Sohn, J. Nucl. Mater. 295 (2001) 213–230.
[25] P. Lovera, C. Ferry, C. Poinssot, L.H. Johnson, Synthesis Report on the Relevant Diffusion Coefficients of Fission Products and Helium in Spent Nuclear Fuels, CEA-R-6039, 2003.
[26] D.C. Parfitt, R.W. Grimes, J. Nucl. Mater. 381 (2008) 216–222.
[27] E. Muller-Casanova, Comportement des gaz de fission dans un combustible irradié lors d'un transitoire de puissance, Thesis – University of Aix-Marseille, 1998.
[28] L. Noirot, J. Nucl. Sci. Technol. 43 (9) (2006) 1149–1160.
[29] David R. Lide (Ed.), Handbook of Chemistry and Physics, 84th ed. CRC Press, 2003-2004. (2003).
[30] N.F. Carnahan, K.E. Starling, J. Chem. Phys. 51 (2) (1969) 635–636.
[31] W.G. Wolfer, High-density equation of state for helium and its application to bubbles in solids, in: H.R. Brager, J.S. Perrin (Eds.), Effects of Radiation on Materials, 10th International Symposium – David Kramer. American Society for Testing and Materials. 1981. p. 201.
[32] W.J. Nellis, N.C. Holmes, A.C. Mitchell, R.J. Trainos, G.K. Governo, M. Ross, D.A. Young, Phys. Rev. Lett. 53 (13) (1984) 1248–1251.
[33] R.O.A. Hall, M.J. Mortimer, D.A. Mortimer, J. Nucl. Mater. 148 (1987) 237–256.
[34] R.B. Stout, C. Ferry, C. Poinssot, J.P. Piron, Estimations of failure pressures in spent fuels from actinide alpha decay helium transported to fission gas bubbles. ICEM'05, in: The 10th International Conference on Environmental Remediation and Radioactive Waste Management, September 4–8, Glasgow, Scotland, 2005.
[35] A.G. Evans, R.W. Davidge, J. Nucl. Mater. 33 (1969) 249–260.
[36] Ph. Garcia, P. Martin, G. Carlot, E. Castelier, M. Ripert, C. Sabathier, C. Valot, F. D'Acapito, J.-L. Hazemann, O. Proux, V. Nassif, J. Nucl. Mater. 352 (2006) 136–143.
[37] J. Spino, K. Vennix, M. Coquerelle, J. Nucl. Mater. 231 (1996) 179–190.
[38] B.R. Lawn, The indentation crack as a model of surface flaw, in: Bradt, Evans, Hasselman, Lange (Eds.), Fracture Mechanics of Ceramics, vol. 5, Plenum Press, New York, London, 1983, p. 692.
[39] Hj. Matzke, J. Spino, J. Nucl. Mater. 248 (1997) 170–179.